# 1.20

# *AB INITIO* STUDY OF MECHANICAL DEFORMATION

Shigenobu Ogata
*Osaka University, Osaka, Japan*

The Mechanical properties of materials under finite deformation are very interesting and are important topics for material scientists, physicists, and mechanical and materials engineers. Many insightful experimental tests of the mechanical properties of such deformed materials have afforded an increased understanding of their behavior. Recently, since nanotechnologies have started to occupy the scientific spotlight, we must accept the challenge of studying these properties in small nano-scaled specimens and in perfect crystals under ideal conditions.

While state-of-the-art experimental techniques have the capacity to make measurements in extreme situations, they are still expensive and require specialized knowledge. However, the considerable improvement in calculation methods and the striking development of computational capacity bring such problems within the range of atomic-scale numerical simulations. In particular, within the past decade, *ab initio* simulations, which can often give qualitatively reliable results without any experimental data as input, have become readily available.

In this section, we discuss methods for studying the mechanical properties of materials using *ab initio* simulations. At present, we have many *ab initio* methods that have the potential to perform such mechanical tests. Here, however, we employ planewave methods based on density functional theory (DFT) and pseudopotential approximations because they are widely used in solid state physics. Details of the theory and of more sophisticated, state-of-the-art techniques can be found in the other section of this volume and in a review article [1]. Concrete examples of parameters settings appearing in this section presuppose that the reader is using the VASP (Vienna *Ab initio* Simulation Package) code [2, 3] and the ultrasoft pseudopotential. Other codes based on the same theory, such as ABINIT, CASTEP, and so on, should basically accept the same parameter settings as on VASP.



*S. Yip (ed.),*
*Handbook of Materials Modeling,* 439–448.

## 1. Applying Deformation to Supercell

In the planewave methods, we usually use a parallelepiped-shaped supercell that has a periodic boundary condition in all directions and includes one or more atoms. The supercell can be defined by three, linearly independent basis vectors, $\boldsymbol{h}_1 = (h_{11}, h_{12}, h_{13})$, $\boldsymbol{h}_2 = (h_{21}, h_{22}, h_{23})$, $\boldsymbol{h}_3 = (h_{31}, h_{32}, h_{33})$. In investigating the phenomena connected with a local atomic displacement, for example, a slip of the adjacent atomic planes in a crystal, an atomic position in the supercell can be directly moved within the system of fixed basis vectors. However, when we need a uniform deformation of the system under consideration, we can accomplish this by changing the basis vectors directly as we would do, for example, in simulating a phase transition or crystal twinning, and in calculations of the elastic constants and ideal strength of a perfect crystal.

Let a deformation gradient tensor $\boldsymbol{F}$ represent the uniform deformation of the system. The $\boldsymbol{F}$ can be defined as

$$F_{ij} = \frac{\mathrm{d}x_i}{\mathrm{d}X_j},$$

where $\boldsymbol{x}$ and $\boldsymbol{X}$ are, respectively, the positions of a material particle in a deformed and in a reference state. By using the $\boldsymbol{F}$, each basis vector is mapped to a new basis vector $\boldsymbol{h}'$ via

$$h'_k = F_{kj} h_j .$$

For example, for a simple shear deformation, $F$ can be written as,

$$\boldsymbol{F} = \begin{pmatrix} 1 & 0 & \gamma \\ 0 & 1 & 0 \\ 0 & 0 & 1 \end{pmatrix},$$

where $\gamma$ represents the magnitude of the shear corresponding to the engineering shear strain. In some cases, for ease of understanding, different coordinate systems for $\boldsymbol{F}$ and for the basis vectors are taken. In this case, $\boldsymbol{F}$ is transformed into the coordinate system for a basis vector by an orthogonal tensor $\boldsymbol{Q}$ ($\boldsymbol{Q}\,\boldsymbol{Q}^T = \boldsymbol{I}$).

$$\boldsymbol{F}' = \boldsymbol{Q}\,\boldsymbol{F}\,\boldsymbol{Q}^T,$$

$$h'_k = F'_{kj} h_j .$$

## 2. Simulation Setting

In DFT calculations, the pseudopotential (if the code is not full-potential code) and the exchange correlation potentials should be carefully selected.

Since these problems are not particular to deformation analysis, the reader who needs a more detailed discussion can find it elsewhere. Only a short commentary is given here.

When we use the pseudopotential in a separable form [4], we need to pay attention to a possible ghost band [5], because almost all DFT codes use the separable form to save computational time and memory resources.

Usually the pseudopotentials in the package codes were very carefully determined to avoid a ghost band in an equilibrium state. However, even when a pseudopotential does not generate a ghost band in the equilibrium state, such a band may still appear in a deformed state. Therefore, it is strongly recommended that a pseudopotential result should be confirmed by comparing it with the result of a full-potential calculation where possible. For the exchange correlation potential, we can normally use functions derived from the local density approximation (LDA), generalized gradient approximation (GGA), and LDA+U. In many cases, the former two methods are equally accurate. The LDA tends to underestimate lattice constants, and overestimate elastic constants and strength, and the GGA to overestimate elastic constants and strength, and underestimate lattice constants. The LDA+U sometimes offers a significantly improved accuracy [6].

The above discussions of the pseudopotential and exchange-correlation potential pertain to error sources resulting from theoretical approximations. However, as well as attending to errors from this source, we should also take care of numerical errors. Numerical errors in the planewave DFT calculation usually derive from the finite size of the $k$-point set and the finite number of planewaves which are uniquely determined by the supercell shape and the planewave cut-off energy. With regard to other problems, a good estimation of the stress tensor to MPa accuracy requires a finer $k$-point sampling than does that for an energy estimation with meV accuracy. Figure 1 shows the

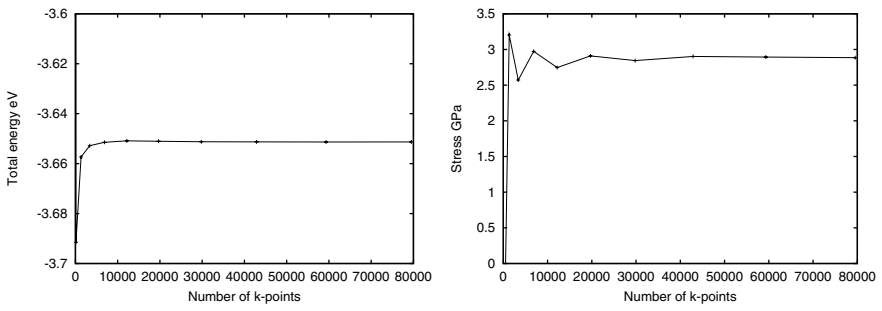


(a) Total energy vs. number of k-points

(b) Shear stress vs. number of k-points

*Figure 1.* Total energy and stress vs. number of $k$-points curves for an aluminum primitive cell under 20% shear in the $\{111\}\langle 11\bar{2}\rangle$ direction.

convergence of the energy and stress as the number of $k$-points is increased. The model supercell is a primitive cell with an fcc structure which contains just one aluminum atom. An engineering shear strain of 0.2 to the $\{111\}\langle 11\bar{2}\rangle$ direction has already been applied to the primitive cell. Only the shear stress component corresponding to the shearing direction is shown. Clearly, the stress converges very slowly even though the energy converges relatively quickly. Figure 2 shows the stress–strain curves of the Al primitive cell under a $\{111\}\langle 11\bar{2}\rangle$ shear deformation using two sets of $k$-points, the normal $15 \times 15 \times 15$ and a fine $43 \times 43 \times 43$ Monkhorst–Pack Brillouin zone sampling [7]. This sampling scheme is explained later. The curve for $15 \times 15 \times 15$ is significantly wavy even though the total free energy of the primitive cell agrees to the order of meV with the energy of the $43 \times 43 \times 43$ case. Apparently, a small set of $k$-points does not produce a smooth stress–strain curve. This is not a small problem for the study of mechanical properties of materials, because, in the above case, the ideal strength, that is, the maximum stress of the stress–strain curve, is overestimated by 20%, a level which is usually corresponds to $2 \sim 20$ GPa.

Although there are many $k$-points sampling schemes, in recent practice, the Monkhorst–Pack sampling scheme is typically used for testing mechanical properties. Since more efficient schemes [8], in which a smaller number

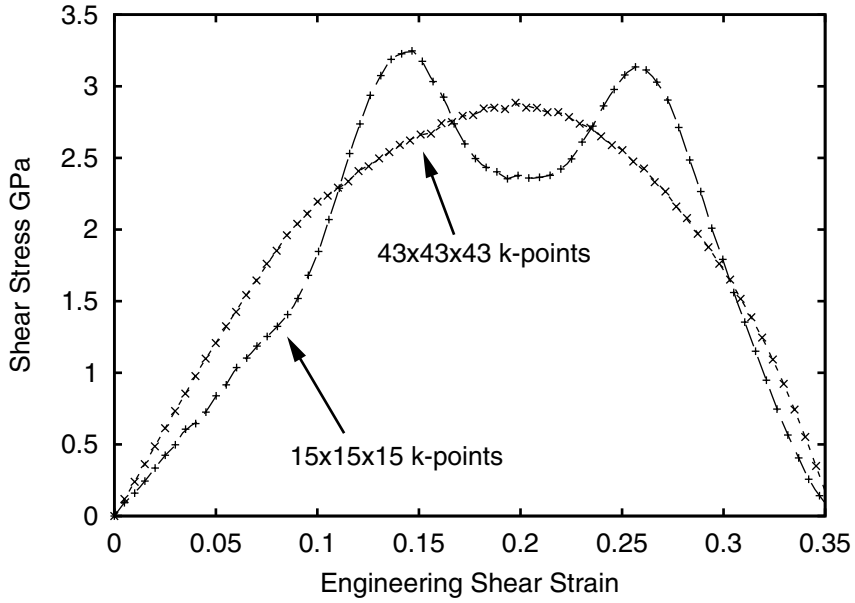


*Figure 2.* Shear stress vs. strain curves calculated with different numbers of $k$-point sets. A shear deformation in the $\{111\}\langle 11\bar{2}\rangle$ direction is applied.

of $k$-points can be used without loss of accuracy, are constructed based on crystal symmetries, a deformation which would break the crystal symmetries would remove their advantage. Therefore, the Monkhorst–Pack scheme is often favored because of its simplicity. In it, the sampling points are defined in the following manner:

$$\boldsymbol{k}(n, m, l) = n\boldsymbol{b}_1 + m\boldsymbol{b}_2 + l\boldsymbol{b}_3,$$
$$n, m, l = \frac{2r - q - 1}{2q}; \quad r = 1, 2, 3, \ldots, q$$

where $\boldsymbol{b}_i$ are the reciprocal lattice vectors of the supercell and $n$, $m$, and $l$ are the mesh sizes for each reciprocal lattice vector direction. Therefore, the total number of sampled $k$-points is $n \times m \times l$. If we find that, under the symmetries of the supercell, some of the $k$-points are equivalent we consider only the nonequivalent $k$-points to save computational time.

The planewave cut-off energy should also be carefully determined. We should use a large enough planewave cut-off energy to achieve a convergence of energy and stress to the required degree of accuracy. Since the atomic configuration affects the cut-off energy, it is better that we estimate that energy for the particular atomic configuration under consideration. However, in mechanical deformation analysis, it is difficult to fix the cut-off energy before starting the simulation because the deformation path cannot be predicted at the simulation's starting point. In such a case, we have to add a safety margin of 10–20 % to the cut-off energy estimated from a known atomic configuration, for example, that of an equivalent structure.

In principle, a complete basis set is necessary to express an arbitrary function by a linear combination of the basis functions. As discussed above, the planewave basis set is used to express the wave functions of electrons in ordinary DFT calculations using the pseudopotential. Because a FFT algorithm can be easily used to calculate the Hamiltonian, we can save computational time. To achieve completeness, a infinite number of the planewaves is necessary; however, to perform a practical numerical calculation, we must somehow reduce the infinite number to a finite one. Fortunately, we can ignore planewaves which have a higher energy than a cut-off value, termed the planewave cut-off energy, because the wave functions of electrons in real system do not have a component of extremely high frequencies.

To estimate the cut-off energy, we can perform a series of calculations with an increasing cut-off energy for a single system. By this means, we can find a cut-off energy which is large enough to ensure that the total energy and the stress convergence of the supercell of interest fall within the required accuracy. Usually, the incompleteness of a finite number of planewave basis sets produces an unphysical stress, that is, a Puley stress. However, by using a large enough number of planewaves, we can avoid this problem. Therefore, both the stress convergence check and the energy convergence check are important in

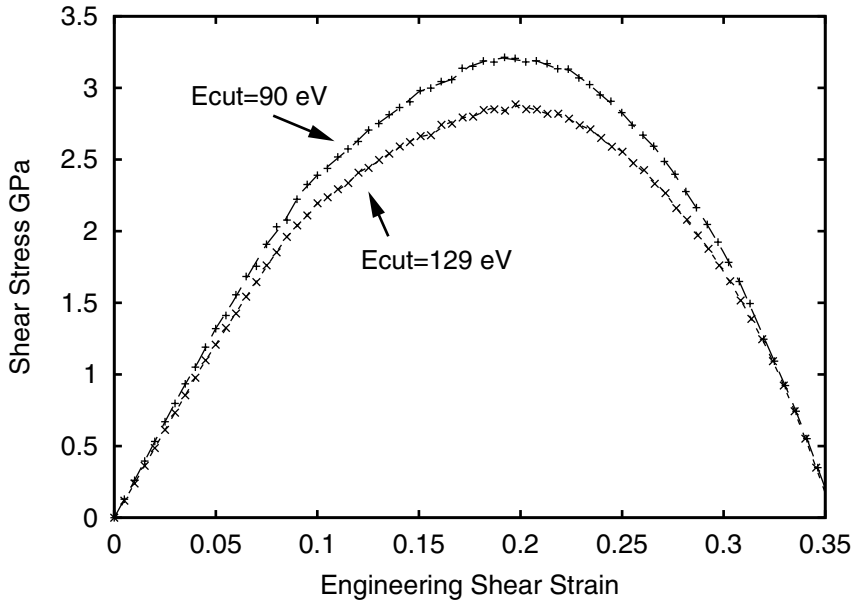


*Figure 3.* Shear stress vs. strain curves calculated with different cut-off energies. A shear deformation in the $\{111\}\langle 11\bar{2}\rangle$ direction is applied.

deformation. Figure 3 shows the stress–strain curves obtained by the use of different planewave cut-off energies. The model and simulation procedure are the same as those we have utilized in the above *k*-point check. Clearly, even though the error due to a small cut-off energy is small in a near equilibrium structure, it becomes larger at in a highly strained structure.

## 3. Mechanical Deformation of Al and Cu

Many *ab initio* studies of mechanical deformation, such as tensile and shear deformation studies for metals and ceramics, have been done in the past two decades. An excellent summary of the history of *ab initio* mechanical testing can be found in a review paper written by Šob [9].

Here, we discuss as examples both a fully relaxed and an unrelaxed uniform shear deformation analysis [10], that is, an analysis of a pure shear and a simple shear, for aluminum and copper. The shear mode is the most important deformation mode in our consideration of the strength of a perfect crystalline solid. The shear deformation analysis usually involves more computational cost than the tensile analysis; because the shear deformation breaks many of the crystal symmetries, many nonequivalent *k*-points should be treated in the calculation.

The following analysis has been performed using the VASP code. The exchange-correlation density functional potential adopted is the Perdew–Wang generalized gradient approximation (GGA) [11]; the ultrasoft pseudopotentials [12] are used. Brillouin zone $k$-point sampling is performed using the Monkhorst–Pack algorithm, and the integration follows the Methfessel–Paxton scheme [13] with the smearing width chosen so that the entropic free energy (a "$-TS$" term) is less than 0.5 meV/atom. A six atom fcc supercell which has three {111} layer is used, and $18 \times 25 \times 11$ $k$-points for Al and $12 \times 17 \times 7$ $k$-points for Cu are adopted. The $k$-point convergence is checked as shown in Table 1. The carefully determined cut-off energies of the planewaves for the Al and Cu supercells are 162 and 292 eV, respectively. Incremental affine shear strains of 1% as described above are imposed on each crystal along the experimentally determined common slip systems to obtain the corresponding energies and stresses. In each step, the stress components, excluding the resolved shear stress along the slip system, are kept to a value less than 0.1 GPa during the simulation.

In Table 2, the equilibrium lattice constants $a_0$ obtained from the energy minimization are listed and compared with the experimental data. The calculated relaxed and unrelaxed shear moduli $G_r$, $G_u$ for the common slip systems are compared with computed analytical values based on the experimental elastic constants. A value of $\Delta\gamma = 0.5\%$ is used to interpolate the resolved shear stress ($\sigma$) versus the engineering shear strain ($\gamma$) curves and to calculate the resolved shear moduli. In the relaxed analysis, the stress components are relaxed to within a convergence tolerance of 0.05 GPa.

*Table 1.* Calculated ideal pure shear $\sigma_r$ and simple shear strengths $\sigma_u$ using different $k$-point sets

| No. of $k$-points | Al | | Cu | |
|---|---|---|---|---|
| | $\sigma^u$ (GPa) | $\sigma^r$ (GPa) | $\sigma^u$ (GPa) | $\sigma^r$ (GPa) |
| $12 \times 17 \times 7$ | 3.67 | 2.76 | 3.42 | 2.16 |
| $18 \times 25 \times 11$ | 3.73 | 2.84 | 3.44 | 2.15 |
| $21 \times 28 \times 12$ | – | – | 3.45 | 2.15 |
| $27 \times 38 \times 16$ | 3.71 | 2.84 | – | – |

*Table 2.* Equilibrium lattice constant ($a_0$), relaxed ($G_r$) and unrelaxed ($G_u$) $\{111\}\langle 11\bar{2}\rangle$ shear moduli of Al and Cu

| | $a_0$ (Å) | $G_r$ (GPa) | $G_u$ (GPa) |
|---|---|---|---|
| Al (calc.) | 4.04 | 25.4 | 25.4 |
| Al (expt.) | 4.03 | 27.4 | 27.6 |
| Cu (calc.) | 3.64 | 31.0 | 40.9 |
| Cu (expt.) | 3.62 | 33.3 | 44.4 |

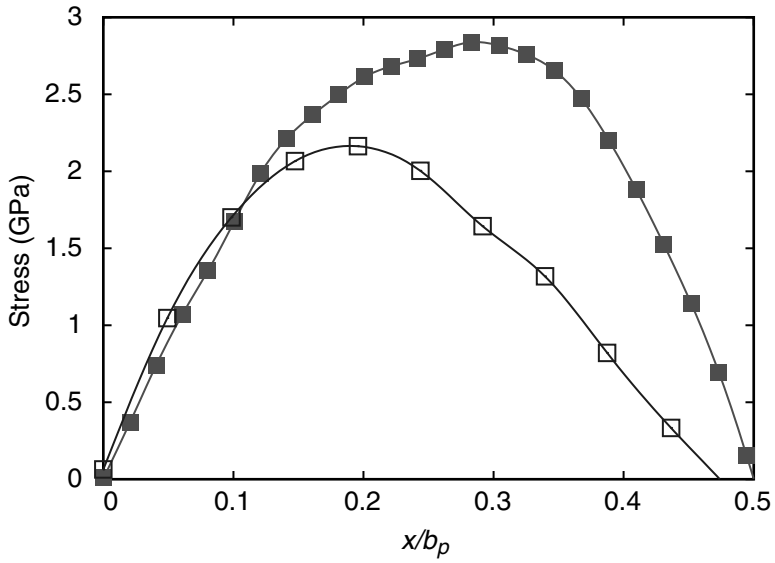


*Figure 4.* Shear stress vs. displacement curves for Al and Cu of the fully relaxed shear deformation in the $\{111\}\langle 11\bar{2}\rangle$ direction.

At equilibrium, the Cu is considerably stiffer, with simple and pure shear moduli greater by 65 and 25%, respectively, than those of the Al. However, the Al ends up with a 32% larger ideal pure shear strength $\sigma_m^r$ than the Cu, because it has a longer range of strain before softening (see Fig. 4): $\gamma_m = 0.200$ in the Al, $\gamma_m = 0.137$ in the Cu.

Figure 5 shows the changes of the iso-surfaces of the valence charge density during the shear deformation ($h \equiv V_{\rm cell}\rho_v$, $V_{\rm cell}$ and $\rho_v$ are the supercell volume and valence charge density, respectively). At the octahedral interstice in Al, the pocket of charge density has cubic symmetry and is angular in shape, with a volume comparable to the pocket centered on every ion. In contrast, in Cu, there is no such interstitial charge pocket, the charge density being nearly spherical about each ion. The Al has an inhomogeneous charge distribution in the interstitial region and bond directionality, while the Cu has relatively homogeneous charge distributions and little bond directionality. The charge density analysis gives a clear view of the electron activity under shear deformation, and sometime informs us about the origin of the mechanical behavior of the solids.

## 4. Outlook

Currently, we can perform *ab initio* mechanical deformation analyses for many types of materials and for primitive and nano systems. However, in the

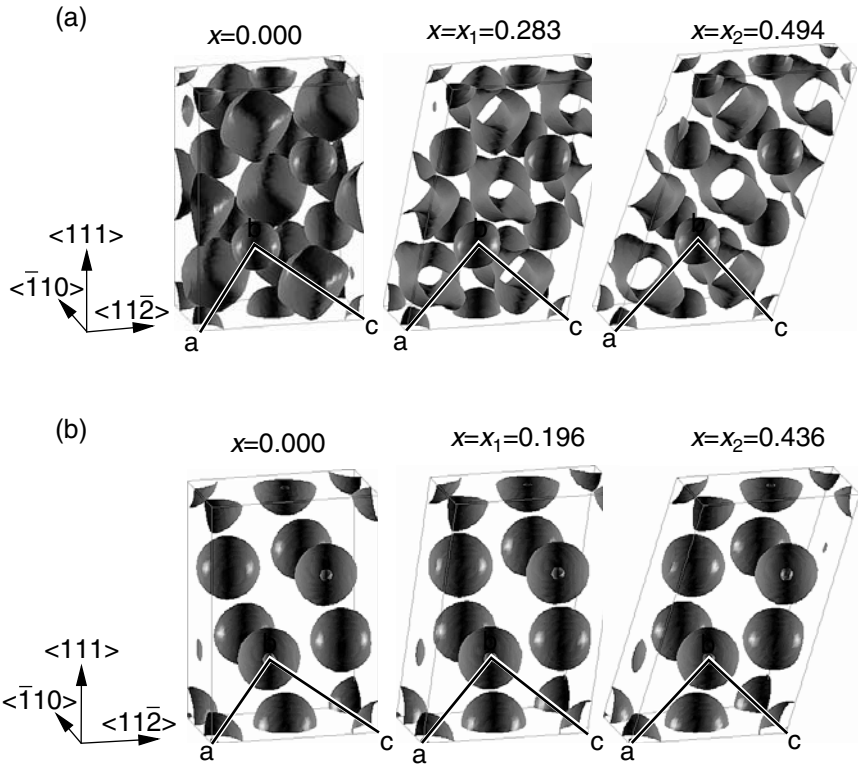


*Figure 5.* Charge density isosurface change in (a) Al; (b) Cu during the shear deformation in the $\{111\}\langle 11\bar{2}\rangle$ direction.

near future, the most interesting studies incorporating these analyses might address not only the mechanical behavior of materials under deformation and loading, but also the relation between mechanical deformation and loading, and physical and chemical reactions, such as stress corrosion. For this purpose, *ab initio* methods are the most powerful and reliable tools.

## References

[1] M.C. Payne, M.P. Teter, D.C. Allan, T.A. Arias, and J.D. Joannopoulos. "Iterative minimization techniques for *ab initio* total-energy calculations – molecular dynamics and conjugate gradients," *Rev. Mod. Phys.*, 64, 1045–1097, 1992.

[2] G. Kresse and J. Hafner, "*Ab initio* molecular dynamics for liquid metals," *Phys. Rev. B*, 47, RC558–RC561, 1993.

[3] G. Kresse and J. Furthmüller, "Efficient iterative schemes for *ab initio* total-energy calculations using a plane-wave basis set," *Phys. Rev. B*, 54, 11169–11186, 1996.

[4] L. Kleinman and D.M. Bylander "Efficacious form for model pseudopotentials," *Phys. Rev. Lett.*, 48, 1425–1428, 1982.

[5] X. Gonze, P. Kackell, and M. Scheffler, "Ghost states for separable, norm-conserving, *ab initio* pseudopotential," *Phys. Rev. B*, 41, 12264–12267, 1990.
[6] S.L. Dudarev, G.A. Botton, S.Y. Savrasov, C.J. Humphreys, and A.P. Sutton, "Electron-energy-loss spectra and the structural stability of nickel oxide: An LSDA+ U study," *Phys. Rev. B*, 57, 1505–1509, 1998.
[7] H.J. Monkhorst and J.D. Pack, "Special points for Brillouin zone integrations," *Phys. Rev. B*, 13, 5188–5192, 1976.
[8] D.J. Chadi, "Special points in the Brillouin zone integrations," *Phys. Rev. B*, 16, 1746–1747, 1977.
[9] M. Šob, M. Friák, D. Legut, J. Fiala, and V. Vitek, "The role of *ab initio* electronic structure calculations," *Mat. Sci. Eng. A*, to be published, 2004.
[10] S. Ogata, J. Li, and S. Yip, "Ideal pure shear strength of aluminum and copper," *Science*, 298, 807–811, 2002.
[11] J.P. Perdew and Y. Wang, "Atoms, molecules, solids, and surfaces: application of the generalized gradient approximation for exchange and correlation," *Phys. Rev. B*, 46, 6671–6687, 1992.
[12] D. Vanderbilt, "Soft self-consistent pseudopotentials in a generalized eigenvalue formalism," *Phys. Rev. B*, 41, 7892–7895, 1990.
[13] M. Methfessel and A. T. Paxton, "High-precision sampling for Brillouin zone in metals," *Phys. Rev. B*, 40, 3616–3621, 1989.